Electronic Supplementary Material (ESI) for Lab on a Chip.
This journal is © The Royal Society of Chemistry 2015

DIAKITE et al.

Point of care diagnostics in ricin exposure

A)

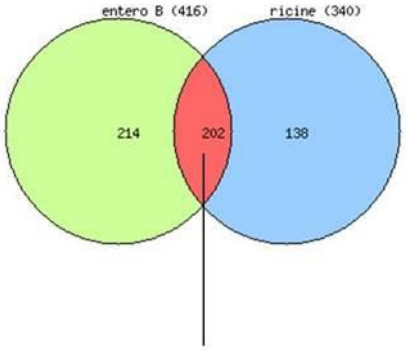

Name	p-value	# Molecules
Inflammatory Response	1,06E-07 - 1,52E-02	40
Cancer	2,60E-06 - 1,52E-02	81
Immunological Disease	2,60E-06 - 1,52E-02	40
Hematological Disease	6,17E-06 - 1,52E-02	42
Hypersensitivity Response	1,61E-04 - 1,52E-02	11

Molecular and Cellular Functions

Name	p-value	# Molecules
Protein Synthesis	4,81E-10 - 3,79E-08	32
Cellular Movement	9,26E-09 - 1,52E-02	51
Cell-To-Cell Signaling and Interaction	1,06E-07 - 1,52E-02	39
Cellular Function and Maintenance	1,06E-07 - 1,52E-02	27
Antigen Presentation	1,88E-06 - 1,52E-02	33

Physiological System Development and Function

Name	p-value	# Molecules
Cell-mediated Immune Response	1,88E-06 - 1,52E-02	36
Humoral Immune Response	1,88E-06 - 1,52E-02	32
Hematological System Development and Function	7,00E-06 - 1,52E-02	37
Immune Cell Trafficking	7,00E-06 - 1,52E-02	26
Tissue Development	1,29E-05 - 1,52E-02	32

B)

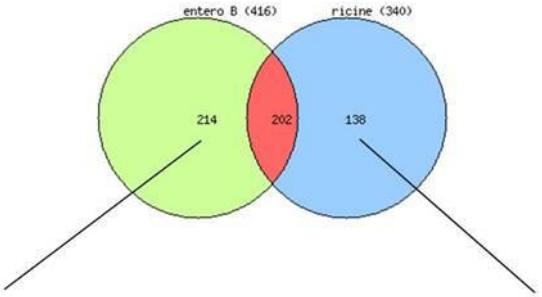

Name	p-value	# Molecules
Organismal Injury and Abnormalities	1,28E-03 - 4,86E-02	4
Infection Mechanism	3,02E-03 - 4,50E-02	10
Cancer	3,49E-03 - 4,39E-02	24
Gastrointestinal Disease	3,49E-03 - 4,86E-02	16
Genetic Disorder	7,70E-03 - 4,38E-02	20

Molecular and Cellular Functions

Name	p-value	# Molecules
Cellular Assembly and Organization	1,07E-04 - 4,38E-02	13
Molecular Transport	2,18E-04 - 4,86E-02	14
Protein Trafficking	2,18E-04 - 1,48E-02	5
Protein Synthesis	5,25E-04 - 4,38E-02	20
RNA Damage and Repair	1,55E-03 - 1,53E-02	3

Physiological System Development and Function

Name	p-value	# Molecules
Cell-mediated Immune Response	6,36E-04 - 4,38E-02	8
Hematological System Development and Function	6,36E-04 - 4,38E-02	20
Tissue Morphology	6,36E-04 - 4,38E-02	7
Cardiovascular System Development and Function	3,14E-03 - 4,39E-02	9
Lymphoid Tissue Structure and Development	4,36E-03 - 4,38E-02	5

Name	p-value	# Molecules
Inflammatory Disease	3,80E-08 - 2,49E-02	31
Immunological Disease	7,54E-08 - 2,49E-02	33
Genetic Disorder	7,65E-07 - 1,66E-02	48
Connective Tissue Disorders	4,14E-06 - 1,66E-02	29
Skeletal and Muscular Disorders	4,14E-06 - 2,49E-02	30

Molecular and Cellular Functions

Name	p-value	# Molecules
Cell Death	6,81E-07 - 2,64E-02	40
Cellular Growth and Proliferation	5,85E-05 - 2,58E-02	45
Cellular Function and Maintenance	2,05E-04 - 2,58E-02	21
Cellular Development	2,30E-04 - 2,74E-02	32
Cellular Assembly and Organization	2,56E-04 - 2,49E-02	20

Physiological System Development and Function

Name	p-value	# Molecules
Hematological System Development and Function	3,23E-04 - 2,49E-02	27
Hematopoiesis	3,23E-04 - 2,49E-02	17
Connective Tissue Development and Function	4,10E-04 - 2,49E-02	13
Nervous System Development and Function	1,01E-03 - 2,49E-02	18
Cell-mediated Immune Response	1,16E-03 - 2,49E-02	22

Figure S1: Mechanism of action of Ricin. The characteristics include inflammation and genes involved in the translation machinery.

Analysis of the kinetics of filling

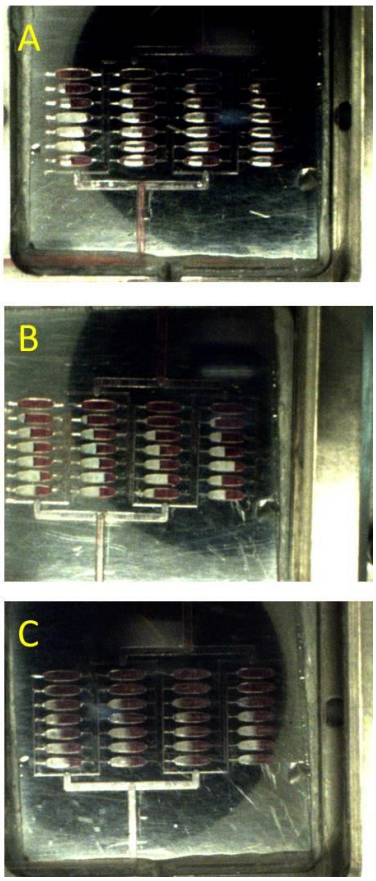

Figure S2: View of the microflows filling the different rows of the RT-qPCR microchambers network for inlet pressure of A) 6000 Pa , B) 300 mbars , and C) 1 bar

It is known that PCR does not accommodate with air bubbles. The parallel filling process of the RT-qPCR microchambers network must be such that no air bubble remains trapped. The main danger is the trapping of bubbles in the microchambers; bubbles in the connecting microchannels downstream from the RT-qPCR microchambers are easily flushed out of the system during filling process. It has been observed that bubbles may form when the flows in the branches of the network are not synchronized. De-synchronization means that a flow arrives before another one at a junction. An example of de-synchronization leading to the formation of bubbles is shown in **Figure S2-A**. Hence, attention must be cast on the synchronization of the flows. In particular, the question rises as to know what must be the inlet pressure in order to maximize flow synchronization. In this section we present an analysis of the inlet pressure effect on the filling process of the device.

Constant cross-section channel

From a physical standpoint, filling of the device is triggered by the pressure of the pressure controller at the inlet and incidentally by the capillary effect on the advancing interfaces in the microchannels. Let us first focus on the inlet pressure. It is recalled that the pressure drop in a microchannel for a laminar flow is given by the general relation

$$\Delta P = RLQ \ , \qquad (1)$$

where P is the pressure, L the channel length, R the hydraulic resistance *per unit length*, and Q the volumic flow rate. Poiseuille and Hagen have given an expression for the resistance R in the case of cylindrical tubes [1,2], Shah and London have derived a Fourier series expression for rectangular duct [3], which has been transformed by Bahrami and colleagues into the following practical expression [4]

$$R = \frac{4\mu}{wd\,\max(w,d)^2}\,q\left(\frac{w}{d}\right), \qquad (2)$$

where q is the form factor defined by

$$q = \frac{1}{3} - \left(\frac{64}{\pi^5}\right)\left(\frac{w}{d}\right)\tanh\left(\frac{\pi}{2\frac{w}{d}}\right). \qquad (3)$$

Relation (1) assumes that the flow is established. Let us consider (1) differently, from a transient point of view, and base our reasoning by considering that the transient flow is always established approximately everywhere. This approximation is valid except at the very front of the advancing flow. Relation (1) can be reinterpreted as

$$P_{in} = RzS\frac{dz}{dt}, \qquad (4)$$

because the pressure at the front end is zero, if we neglect the capillary Laplace pressure, and P_{in} at the back end (inlet pressure). In (4), S is the cross section area of the channel and z the instantaneous penetration length. Integration of (4) yields

$$z = \sqrt{\frac{2\,P_{in}}{R\,S}\,t}\,. \qquad (5)$$

The penetration distance varies as the square root of time. The timer taken for filling the complete channel is then

$$\tau = \frac{z^2\,R\,S}{2\,P_{in}}. \qquad (6)$$

Piecewise constant cross-section channel

Relation (6) has been developed for a constant cross-section channel. Now, consider a piecewise constant cross-section channel and rewrite (1) as

$$\Delta P = \left(\sum RL\right)\,Q\,. \qquad (7)$$

Using the same approach as before, assuming n sections of length L_i, i=1,n, with the liquid front in the n^{th} channel, as shown in **Figure S3-A**, we obtain the relation

$$P_{in} = \left(\sum_{i=1}^{n-1} R_i\,L_i + R_n\left(z - \sum_{i=1}^{n-1} L_i\right)\right) S_n\,\frac{dz}{dt}\,. \qquad (8)$$

Integration of (8) yields

$$t - \sum_{i=1}^{n-1} \tau_i = \frac{S_n}{P_{in}} \left[\sum_{i=1}^{n-1} R_i \, L_i (z - \sum_{i=1}^{n-1} L_i) + \frac{R_n}{2} (z - \sum_{i=1}^{n-1} L_i)^2 \right],$$
(9)

where τ_i are the times for the flow to totally cross the channel i. The time lapse τ_n is then

$$\tau_n = \frac{L_n \, S_n}{P_{in}} \left[\sum_{i=1}^{n-1} R_i \, L_i + \frac{R_n}{2} L_n \right] . \qquad (10)$$

The flow front reaches the end of the n^{th} channel at the time

$$t_n = \sum_{i=1,n}^{n} \tau_i \ . \qquad (11)$$

We obtain an important result: Substitution of (10) in (11) indicates that the time t_n is inversely proportional to P_{in}.

Synchronization analysis

Now for simplicity, consider two channels consisting of only two different cross sections (**Figure S3-B**). Analysis of the synchronization at the junction (P_{out}) can be done by using a configuration of the two parallel channels where the sections have been permuted. The time required for the flow to reach the extremity of first system is

$$t_{1,2} = \tau_1 + \tau_2 = \frac{L_1 \, S_1}{P_{in}} \left[\frac{R_1}{2} \, L_1 \right] + \frac{L_2 \, S_2}{P_{in}} \left[R_1 \, L_1 + \frac{R_2}{2} \, L_2 \right] . \quad (12)$$

On the other hand, in the second system

$$t_{2,1} = \tau_2^* + \tau_1^* = \frac{L_2 \, S_2}{P_{in}} \left[\frac{R_2}{2} \, L_2 \right] + \frac{L_1 \, S_1}{P_{in}} \left[R_2 \, L_2 + \frac{R_1}{2} \, L_1 \right] . \quad (13)$$

The two different geometries are not commutative: the time required to reach the channel outlet depends on the history of the flow in all the sections. The de-synchronization time is

$$\Delta t_{1,2} = t_{1,2} - t_{2,1} = \frac{L_1 \, L_2}{P_{in}} \, (S_2 \, R_1 - S_1 \, R_2) . \qquad (14)$$

Figure S3-C shows the kinetics of liquid progression in each twin systems and the resulting de-synchronization. Using relation (14), it is possible to know which one of the two flows will arrive first. Let us write

$$sign \, (t_{1,2} - t_{2,1}) = sign(S_2 \, R_1 - S_1 \, R_2) = sign(\frac{R_1}{S_1} - \frac{R_2}{S_2}) . \quad (15)$$

If S_1 is a small cross section and conversely S_2 is a large cross section, R_1 has a high value and R_2 has a low value. According to **Figure S3-B**, it is straightforward to see that $\frac{R_1}{S_1} \gg \frac{R_2}{S_2}$ and the flow in channel (1) will arrive later that the flow in channel (2). The de-synchronization time is then important. The larger the contrast in the cross section area between the two sections of a same system, the larger the de-synchronization. Logically, systems with small contrast in cross-section do not show much de-synchronization. However, increasing the inlet pressure P_{in} considerably reduces the de-synchronization. A sufficient inlet pressure reduces enough the de-synchronization time to have the RT-qPCR microchambers filled without trapping bubbles.

This result can be seen in **Figure S2-B and C**, where the system is partly synchronized (in the first rows) for P_{in} =300 mbars, and completely synchronized for P_{in}=1 bar. The synchronization is clearly seen in **Figure S2-C**, where the different advancing interfaces in the chambers are delayed from a nearly constant time.

From the previous analysis, the rows should fill sequentially from the top, where then main channel connected to the pressure controller meets the network. This property can be deduced from (14) by increasing L_2, while all the other parameters stay constant. Synchronization level decreases from row to row.

This remark raises the question as to why the very low inlet pressure case (6000 Pa) is so much de-synchronized, without following any sequential progression. We suggest a capillary effect. The channel walls have a contact angle with water of approximately 60° and the cover film contact angle is 20°. The generalized Cassie angle derived in [4] is approximately 45°. Hence a very approximate magnitude of the capillary pressure is

$$P_{cap} \cong 1.4 \ \frac{\gamma}{D_H}, \qquad (16)$$

where D_H is the hydraulic diameter of the channel. Note that the Laplace pressure is negative because of the concavity of the interface. Numerically, P_{cap} ~ 1000-2000 Pa for the smaller section channels, and only 150 in the microchambers. The value of P_{cap} is not negligible compared to the inlet pressure P_{in}= 6000 Pa in the small section channels. Conversely, the capillary effect is negligible in the large PCR chambers. In a small channel, when the inlet pressure is small, relation (4) must be rewritten under the form

$$P_{in} - P_{cap} = RzS\frac{dz}{dt}. \qquad (17)$$

where P_{cap} is negative. Hence, the flow accelerates in the small section channels more than in the large section channels. The de-synchronization effect increases, as shown in **Figure S2-D**. In **figure S2-D**, we can see that the flow has arrived at the exit junction in the branch (2) while the flow is just penetrating the larger section of branch (1). In our complete system, once the first RT-qPCR microchamber is filled (at the top) the flow continues quickly and reaches the exit before the other flows have penetrated in their PCR chambers (**Figure S2-A**). Back flows appear in the other rows and bubbles are trapped, as shown in the **Figure S3-E-C**.

In conclusion, very small inlet pressures lead to unstable filling due to a combine capillary-forced flow effect, medium range inlet pressures assure the synchronization of the first rows only, and relatively large inlet pressures are needed to have the whole network synchronized. Although not demonstrated here, the analytical formulation has been established for a network with two branches only, but can be extrapolated to more complicated networks. However, in this case, the approach to produce a closed form formulation is very cumbersome and requires complicated algebra.

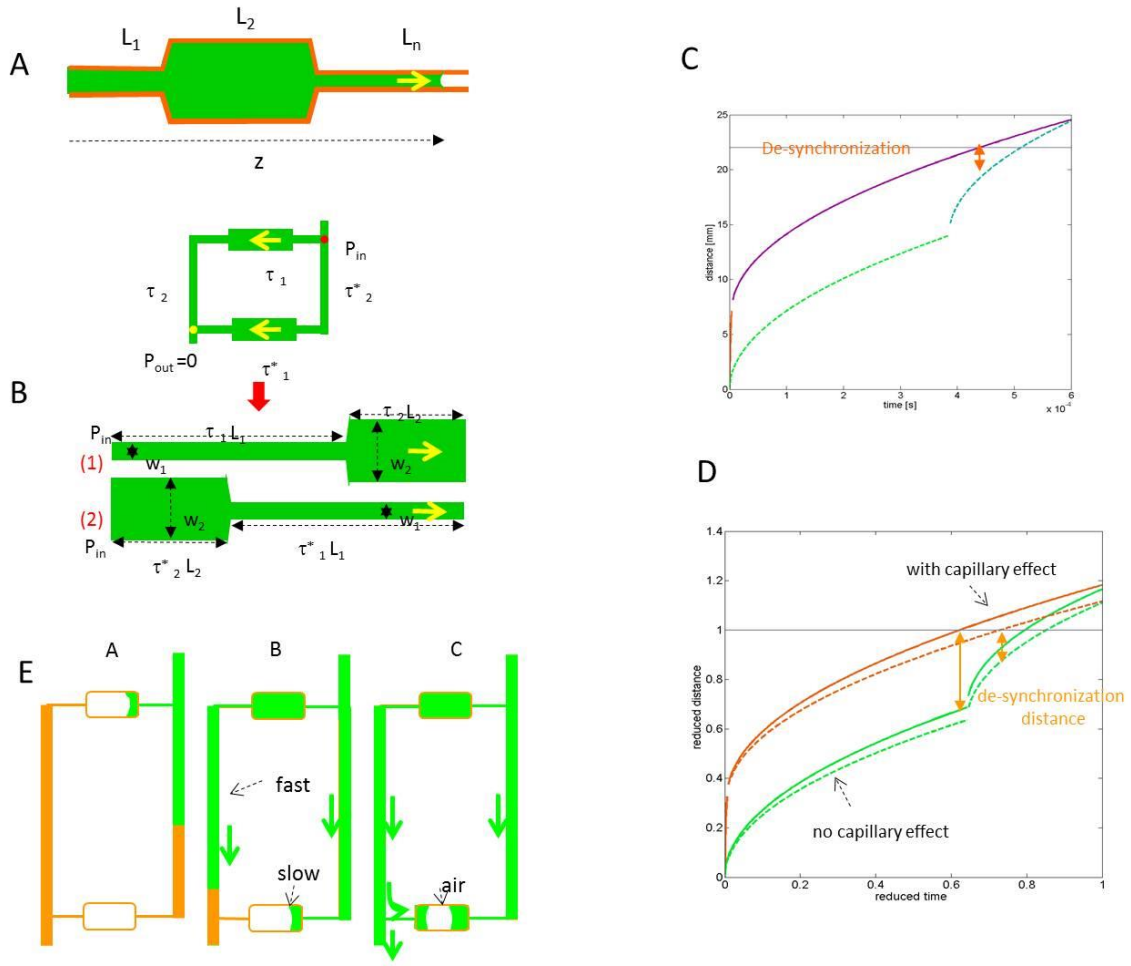

Figure S3: A) Sketch of a piecewise constant cross-section channel. B) Top: sketch of the two fluid paths; bottom: two channel systems with permuted sections. C) Progression of the liquid in each channel according to the model: the liquid that starts with the larger section arrives first. De-synchronization produces delay of around 2 mm at the junction. D) De-synchronization is increased by the effect of the capillary pressure at the tip of the flow: orange curves correspond to the system (2) of **figure S3-B,** and green to the system (1); the dots indicate that capillary is ignored, and the continuous lines are obtained with the complete model. E) Combination of pumping and capillary effects: A, the flow starts invading the network; B, once the flow has past the first chamber at the top, it accelerates downwards ("fast" on the figure); C, the flow penetrates the bottom chamber by the two sides, trapping air.

References

[1] H. Bruus. Theoretical microfluidics, Oxford University Press, 2007.
[2] J. Berthier, P. Silberzan. Microfluidics for biotechnology, 2nd edition, Artech House publishing, 2012.
[3] R.K. Shah, A.L. London. Laminar flow forced convection in ducts, Supplement 1 to Advances in Heat Transfer (New York: Academic Press), 1978.
[4] M. Bahrami, M. M. Yovanovich and J. R. Culham, Pressure Drop of Fully-Developed, Laminar Flow in Microchannels of Arbitrary Cross-Section, J. Fluids Eng. 128(5), 1036-1044, 2006.
[5] J. Berthier, K. Brakke, E. Berthier, A general condition for spontaneous capillary flow in uniform cross-section microchannels. Microfluid. Nanofluid. Journal, 16(4), 779-785,2014.

Detailed description of the device operation

Suspensions for mRNA isolation

The protocol for mRNA isolation from blood was similar to the standard protocol of the mRNA DIRECT™ Kit (Life Technologies, France). It used the reagents of the DIRECT™ Kit, including the Dynabeads® oligo-DT suspension, washing buffers A and B, and the lysis binding buffer.

The lysis/binding suspension was prepared by mixing 150 µl of lysis/binding buffer, 30 µl of mouse blood collected in a Paxgene Tube (equivalent of 10 µl whole blood), and 6 µl of dynabeads® oligo-DT. After mixing, the suspension was allowed to stand for 3 minutes before use to allow for mRNA capture on the beads. During this waiting step, the mixture was vortexed every 30 sec. The blood in collected a Paxgene tube was also vortexed before use in preparing the suspension for lysis/binding.

RT-qPCR reactions

The suspension for the RT-qPCR reactions was based on the SuperScript® III Platinum® One-Step qRT-PCR kit (Life Technologies, France), with the following optimized reagent concentrations: 1X Reaction Mix, 3rxn of Superscript III RT/platinum Taq Mix, 300 units of RNaseOUT™ Recombinant Ribonuclease Inhibitor (Life Technologies, France) and 2 mM magnesium (Life technologies, France).

Step	Description	Applied Pressure (mbar)	Valve actuation scheme	Time (Sec)
1	Injection of the mixture for Lysis/Binding in the sample preparation chamber.	**20**	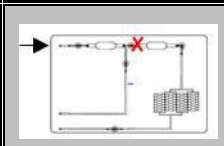	**25**
2	Isolation of the bead/mRNA complex in the chamber using the magnet.		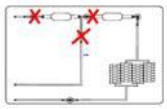	**60**
3	Flush the chamber with air. The magnet maintains the bead/mRNA complex.	**end 700** **20 start**	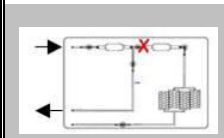	**45**
4	Injection of buffer A. The magnet maintains the bead/mRNA complex.	**20**	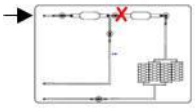	**25**

5	Removal of the magnet and mixing of mRNA/bead complex with buffer A using the mechanical mixer.		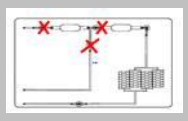	**60**
6	Repeat once step 2 and step 5.			**215**
7	Flush the chamber with air. The magnet maintains the bead/mRNA complex.	**end 700** **20 start**	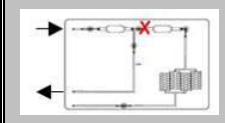	**45**
8	Injection of buffer B. The magnet maintains the bead/mRNA complex.	**20**	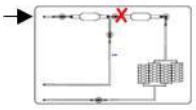	**25**
9	Removal of the magnet and mixing of mRNA/bead complex with buffer B using the mechanical mixer.		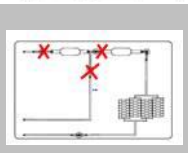	**60**
10	Repeat once step 2 and step 3.			**105**
11	Injection of the suspension for RT-qPCR. The magnet maintains the bead/mRNA complex.	**20**	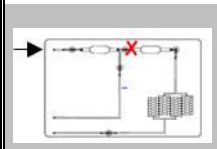	**25**
12	Removal of the magnet and mixing of mRNA/bead complex with the suspension for RT-qPCR using the mechanical mixer.	**end 700** **20 start**	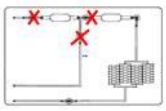	**60**
13	Push the mixture into the prefilling chamber and stop when the chamber is ¾ filled.	**20**	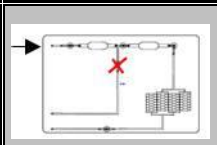	**10**
14	Push the mixture into the RT-qPCR chambers (rapid and simultaneous filling of 4X7 RT-qPCR chambers).	**1000**	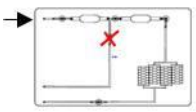	**0.7**
15	Run RT-qPCR thermal cycling.		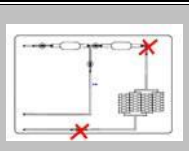	

The sample preparation takes approximately 13 min, and the 40 cycles for RT-qPCR last approximately 67 min (15 min 7 s for RT reaction and 52 min for PCR reaction), for a total of approximately 80 min for the entire process.